Geophys. J. R. astr. Soc. (1982) **69**, 121–135

The growing spherical seismic source

Jeffry L. Stevens* *Cooperative Institute for Research in Environmental Sciences, University of Colorado/NOAA, Boulder, Colorado 80309, USA*

Received 1981 August 6; in original form 1980 September 22

Summary. A solution is found for the seismic radiation from an arbitrarily growing spherical source in an inhomogeneously prestressed elastic medium. The general problem of the growing seismic source in a prestressed medium is formulated as a boundary value problem. For the special case of the growing spherical source, an expansion in vector spherical harmonics reduces the problem to a set of one-dimensional Volterra integral equations. The equations can be easily formed through the use of Bessel function recursion relations. The integral equations for a growing spherical cavity are solved numerically. Waveforms are then computed for homogeneous and inhomogeneous stress fields for several growth histories. The resulting waveforms are similar to the waveforms of the corresponding instantaneous problem, but stretched out in time and reduced in amplitude. The effects of diffraction and the overshoot of equilibrium are reduced with a reduction in growth rate. The effects caused by inhomogeneity of the stress field are quite strong for the growing as well as for the instantaneous seismic source.

1 Introduction

Spherical sources have been used a number of times in the past as models for earthquakes and for the tectonic release from explosions. The spherical source problem can be solved under a very wide range of conditions, so it forms an important canonical problem for the general seismic source problem. Nearly all exact solutions to spherical problems have been for an instantaneous change in material properties. Hirasawa & Sato (1963) computed the seismic radiation from the sudden creation of a spherical cavity in a uniform shear stress field. Koyama, Horiuchi & Hirasawa (1973) computed the seismic radiation from a region which suddenly changes to a fluid in a uniform shear field. Stevens (1980a) computed the seismic radiation from the sudden creation of a spherical cavity in an arbitrarily prestressed medium and studied the effects of local stress concentrations. The instantaneous problems are relatively simple since the problems can be solved by applying Fourier or Laplace transform techniques. Time-dependent problems are more difficult since they must be solved in the time domain.

*Now at Systems, Science and Software, PO Box 1620, La Jolla, California 92038, USA.

It is important to consider the effects of finite growth rate, since for earthquakes the rupture growth must always be subsonic. Even for nuclear explosions, some time will be required for the creation of the cavity and the growth rate may be subsonic. Stevens (1980a) found a number of anomalous effects which appear when failure occurs instantaneously in an inhomogeneously prestressed medium. Observation of these effects could lead to the identification of stress concentrations in the Earth, but they might be masked by growth effects. One purpose of this paper is to study the effect of a finite growth rate in addition to an inhomogeneous prestress field.

A major advantage of the spherical geometry is that the vector elastic equations separate in spherical coordinates. Even for time-dependent problems, the equations can be reduced to a set of one-dimensional differential or integral equations. The only previous solutions to growing source problems are for a uniformly growing cavity (Burridge & Alterman 1972) and for a uniformly growing cavity which suddenly stops (Burridge 1975). Both of these solutions are valid only for a uniform shear field. In principle these solutions can be extended to the general case (arbitrary growth rates and arbitrary stress fields), but this involves a great deal of tedious algebra and requires solving a number of sets of high order differential equations (Stevens 1980b).

Archambeau (1972), Minster & Suteau (1977), and Minster (1979) have used an approximate solution for a growing spherical source in a uniform shear stress field as a model for the tectonic release from explosions. This 'transparent source approximation' uses an infinite space Green's function to propagate the effect of the change in prestress caused by the material transformation, but neglects the effect of the surface itself. In this paper we avoid the problems which occur with the approximate solutions by satisfying boundary conditions on the growing surface.

By expanding the unknown displacement field in vector spherical harmonics the growing source problem can be reduced to a set of one-dimensional integral equations which can be solved numerically. The amount of algebra required is greatly reduced through the use of Bessel function recursion relations. Formulation of the integral equations is then straightforward even for complex prestress fields.

2 Formulation of the problem

We need to solve the elastic equations in a prestressed medium subject to the boundary condition of conservation of momentum on the growing boundary. The elastic operator is defined by

$$L_{il}u_l = \frac{\partial}{\partial x_j} C_{ijkl} \frac{\partial}{\partial x_k} u_l. \tag{2.1}$$

The initial displacement field $\mathbf{u}^0$ (referenced to a state with no prestress) satisfies

$$L_{ij}u_j^0 = -f_i(x) \tag{2.2}$$

where f_i represents the static body force density. We define the total displacement $\mathbf{u}^t$ and the dynamic displacement $\mathbf{u}$ by

$$\mathbf{u}^t = \mathbf{u}^0 + \mathbf{u}. \tag{2.3}$$

The total displacement satisfies

$$\mathbf{L} \cdot \mathbf{u}^t - \rho \frac{\partial^2}{\partial t^2} \mathbf{u}^t = -\mathbf{f}(x) \tag{2.4}$$

assuming there are no time-dependent body forces (ρ is the density). The dynamic displacement field therefore satisfies

$$\mathbf{L}\cdot\mathbf{u} - \rho\frac{\partial^2}{\partial t^2}\mathbf{u} = 0. \tag{2.5}$$

The displacement field $\mathbf{u}$ is zero initially and becomes non-zero after the formation of the failure zone. It satisfies the elastic equations with inhomogeneous boundary conditions. Conservation of momentum across the moving boundary is given by (Archambeau & Minster 1978):

$$\left[\!\left[\mathbf{T}(\mathbf{u}^t) + \rho\frac{\partial \mathbf{u}^t}{\partial t}\mathbf{U}\right]\!\right]\cdot\hat{n} = 0 \tag{2.6}$$

where $\mathbf{T}$ is the stress operator defined by

$$[\mathbf{T}(\mathbf{u})]_{ij} = C_{ijkl}\frac{\partial}{\partial x_k}u_l \tag{2.7}$$

and $\mathbf{U}$ is the rupture velocity. The brackets $[\![\ ]\!]$ indicate the change in the quantity across the boundary. If the material inside the source region becomes very weak, then $C_{ijkl} \approx 0$ inside. Using this condition and equation (2.3) we find the boundary condition for the dynamic displacement field $\mathbf{u}$ to be:

$$\mathbf{T}(\mathbf{u})\cdot\hat{n} + \left[\!\left[\rho\frac{\partial \mathbf{u}}{\partial t}\right]\!\right]\mathbf{U}\cdot\hat{n} = -\mathbf{T}(\mathbf{u}^0)\cdot\hat{n}. \tag{2.8}$$

In general the jump in velocity (and density) across the boundary is not known, however, Burridge (1976) has shown that if the density remains constant across the boundary (as required by the linear theory) and the energy of transformation at the boundary is dissipated as heat, then

$$\left[\!\left[\frac{\partial \mathbf{u}}{\partial t}\right]\!\right] = 0 \tag{2.9}$$

and the second term in (2.8) vanishes. We will usually assume this condition, but will consider the effect of this extra term later on. Under this condition the boundary condition becomes:

$$\mathbf{T}(\mathbf{u})\cdot\hat{n} = -\mathbf{T}(\mathbf{u}^0)\cdot\hat{n} \tag{2.10}$$

so the problem is equivalent to a stress pulse equal to minus the initial prestress applied to the (growing) cavity surface.

The assumption that $C_{ijkl} \approx 0$ inside is of course an over-simplification of the problem. Within the limits of linear theory, however, we cannot consider density changes or convection, nor a material which may be strong in compression but very weak in tension. It is possible to extend the problem to include a linear material inside by using internal eigenvectors for this material and requiring continuity of normal (and tangential for a solid) displacements across the surface (Koyama *et al.* 1973; Stevens 1980b), but this is a much more restrictive condition than is likely to result from the crushed and cracked material in a real physical process. In addition to this, it is not clear what initial conditions to place on the transformed material without a detailed study of the failure process. For these reasons, the stress free boundary condition (equation 2.8) seems to be the best idealization of the seismic source without including non-linear effects.

3 Separation of the differential equations – spherical eigenvectors

The elastic equations separate in spherical coordinates by introducing vector spherical harmonics. The orthogonal vectors $\mathbf{P}_{lm}$, $\mathbf{B}_{lm}$ and $\mathbf{C}_{lm}$ as defined by Ben-Menahem & Singh (1968) are:

$$\mathbf{P}_{lm} = \hat{e}_r Y_{lm}(\theta, \phi)$$

$$\sqrt{l(l+1)}\,\mathbf{B}_{lm} = \left[\hat{e}_\theta \frac{\partial}{\partial\theta} + \frac{\hat{e}_\phi}{\sin\theta}\frac{\partial}{\partial\phi}\right] Y_{lm}(\theta, \phi) \tag{3.1}$$

$$\sqrt{l(l+1)}\,\mathbf{C}_{lm} = \left[\hat{e}_\theta \frac{1}{\sin\theta}\frac{\partial}{\partial\phi} - \hat{e}_\phi \frac{\partial}{\partial\theta}\right] Y_{lm}(\theta, \phi)$$

where Y_{lm} is the spherical harmonic defined by

$$Y_{lm}(\theta, \phi) = P_{lm}(\cos\theta)\exp(im\phi)$$

and the associated Legendre function is defined by

$$P_{lm}(x) = \frac{1}{2^l l!}(1-x^2)^{m/2}\frac{d^{l+m}}{dx^{l+m}}(x^2-1)^l. \tag{3.2}$$

As shown in the Appendix, these vectors are equivalent to the generalized spherical harmonics defined by Burridge (1969) and used by Burridge & Alterman (1972) to solve a similar problem.

A general solution to the elastic equations at any point in the medium external to the cavity can be written in the frequency domain in the form:

$$\mathbf{u}(\mathbf{x}, \omega) = \sum_{l=0}^{\infty}\sum_{m=-l}^{l} d^1_{lm}(\omega)\,\mathbf{L}^-_{lm} + d^2_{lm}(\omega)\,\mathbf{N}^-_{lm} + d^3_{lm}(\omega)\,\mathbf{M}^-_{lm} \tag{3.3}$$

where

$$\begin{aligned}
\mathbf{M}^-_{lm} &= g^{1-}_l(\omega r/\beta)\,\mathbf{C}_{lm}(\theta, \phi)\\
\mathbf{N}^-_{lm} &= g^{2-}_l(\omega r/\beta)\,\mathbf{P}_{lm}(\theta, \phi) + g^{3-}_l(\omega r/\beta)\,\mathbf{B}_{lm}(\theta, \phi)\\
\mathbf{L}^-_{lm} &= g^{4-}_l(\omega r/\beta)\,\mathbf{P}_{lm}(\theta, \phi) + g^{5-}_l(\omega r/\alpha)\,\mathbf{B}_{lm}(\theta, \phi).
\end{aligned} \tag{3.4}$$

These represent toroidal, spheroidal shear and spheroidal compressional waves respectively. The functions g^{i-}_l are defined by Stevens (1980a) and are linear combinations of spherical Hankel functions similar to the time domain equivalents which will be defined by equation (3.15).

The method of solution to the problem of the growing spherical cavity is to transform equation (3.3) and the associated tractions to the time domain and match the boundary condition (equation 2.8) as a function of time on the growing boundary. The coefficients d^i_{lm} in the time domain will be the solution to the problem.

The next step is to define the function

$$H^-_{ln}(r, t) = \frac{1}{2\pi}\int_{-\infty}^{\infty} d\omega\,\omega^n h^{(2)}_l\left(\frac{\omega r}{v}\right). \tag{3.5}$$

This function will appear with $n = 0$ for the displacements and $n = 1$ for the tractions and velocities. The spherical Hankel function $h^{(2)}_l$ can be written in the form

$$h^{(2)}_l\left(\frac{\omega r}{v}\right) = \exp(-i\omega r/v)\,P^l\left(\omega\frac{r}{v}\right) \tag{3.6}$$

where the P^l are polynomials with coefficients which can be determined from the recursion relations for spherical Bessel functions.

We define

$$P^l(\omega x) = \sum_{s=1}^{l+1} a_l^s \frac{1}{(\omega x)^s}. \tag{3.7}$$

For any Bessel function $Z_l(x)$, a recursion relation is

$$Z_{l+1} = \frac{2l+1}{x} Z_l - Z_{l-1}. \tag{3.8}$$

So the coefficients in (3.7) are determined by:

$$a_l^s = (2l-1)\, a_{l-1}^{s-1} - a_{l-2}^s \tag{3.9}$$

with the first coefficient given by $a_0^1 = i$. Useful special cases are:

$$\begin{aligned} a_l^1 &= i^{l+1} \\ a_l^l &= i(2l-1)!! \\ a_l^{l+1} &= -(2l-1)!!. \end{aligned} \tag{3.10}$$

We can now rewrite (3.5) in the form (letting $x = r/v$):

$$H_{ln}^- = \sum_{s=1}^{l+1} \frac{a_l^s}{x^s} i^{s-n} \frac{1}{2\pi} \int_{-\infty}^{\infty} d\omega \frac{\exp[i\omega(t-x)]}{(i\omega)^{s-n}}. \tag{3.11}$$

Evaluating the time domain function:

$$\boxed{H_{ln}^- = \delta_{n1} \frac{a_l^1}{x} \delta(t-x) + \sum_{s=n+1}^{l+1} a_l^s \frac{i^{s-n}}{x^s} \frac{(t-x)^{s-n-1} H(t-x)}{(s-n-1)!}}. \tag{3.12}$$

The displacements in the time domain can now be written in the form:

$$\mathbf{u}(\mathbf{x}, t) = \int_{-\infty}^{\infty} d\tau \left[d_{lm}^1(\tau)\, \mathbf{L}_{lm}^-(t-\tau) + d_{lm}^2(\tau)\, \mathbf{N}_{lm}^-(t-\tau) + d_{lm}^3(\tau)\, \mathbf{M}_{lm}^-(t-\tau) \right] \tag{3.13}$$

where

$$\begin{aligned} \mathbf{M}_{lm}^-(t) &= \tilde{g}_l^{1-}(t - r/\beta)\, \mathbf{C}_{lm} \\ \mathbf{N}_{lm}^-(t) &= \tilde{g}_l^{2-}(t - r/\beta)\, \mathbf{P}_{lm} + \tilde{g}_l^{3-}(t - r/\beta)\, \mathbf{B}_{lm} \\ \mathbf{L}_{lm}^-(t) &= \tilde{g}_l^{4-}(t - r/\alpha)\, \mathbf{P}_{lm} + \tilde{g}_l^{5-}(t - r/\alpha)\, \mathbf{B}_{lm} \end{aligned} \tag{3.14}$$

and:

$$\begin{aligned} \tilde{g}_l^{1-} &= \sqrt{l(l+1)}\, i^l H_{l,0}^- && v = \beta \\ \tilde{g}_l^{2-} &= \frac{l(l+1)}{2l+1} i^{l+1} (H_{l-1,0}^- + H_{l+1,0}^-) && v = \beta \\ \tilde{g}_l^{3-} &= \frac{\sqrt{l(l+1)}}{2l+1} i^{l+1} [(l+1) H_{l-1,0}^- - l H_{l+1,0}^-] && v = \beta \\ \tilde{g}_l^{4-} &= \frac{1}{2l+1} i^{l+1} [l H_{l-1,0}^- - (l+1) H_{l+1,0}^-] && v = \alpha \\ \tilde{g}_l^{5-} &= \frac{\sqrt{l(l+1)}}{2l+1} i^{l+1} (H_{l-1,0}^- + H_{l+1,0}^-) && v = \alpha. \end{aligned} \tag{3.15}$$

The associated velocities are the inverse transforms of the same functions multiplied by $i\omega$. Thus the velocities corresponding to g_l^{1-} have the same form except for a factor of i and the index $n = 1$.

Similarly, the associated tractions are given by

$$\mathbf{T}(\mathbf{u})\cdot\hat{n} = \int_{-\infty}^{\infty} d\tau \,[\![d_{lm}^1(\tau)\,[\mathbf{T}(\mathbf{L}_{lm}^-)(t-\tau)] + d_{lm}^2(\tau)\,[\mathbf{T}(\mathbf{N}_{lm}^-)(t-\tau)] + d_{lm}^3(\tau)\,[\mathbf{T}(\mathbf{M}_{lm}^-)(t-\tau)]\,]\!] \tag{3.16}$$

where

$$\begin{aligned}
\mathbf{T}(\mathbf{M}_{lm}^-) &= h_l^{1-}(t-r/\beta)\,\mathbf{C}_{lm}\\
\mathbf{T}(\mathbf{N}_{lm}^-) &= h_l^{2-}(t-r/\beta)\,\mathbf{P}_{lm} + h_l^{3-}(t-r/\beta)\mathbf{B}_{lm}\\
\mathbf{T}(\mathbf{L}_m^-) &= h_l^{4-}(t-r/\alpha)\,\mathbf{P}_{lm} + h_l^{5-}(t-r/\alpha)\,\mathbf{B}_{lm}
\end{aligned} \tag{3.17}$$

and

$$\begin{aligned}
\tilde{h}_l^{1-} &= \frac{\mu}{\beta}\frac{\sqrt{l(l+1)}\,i^l}{2l+1}\,[(l-1)H_{l-1,1}^- - (l+2)H_{l+1,1}^-]\\
\tilde{h}_l^{2-} &= \frac{\mu}{\beta}\frac{2l(l+1)\,i^{l+1}}{(2l-1)(2l+1)(2l+3)}\,[(l-1)(2l+3)H_{l-2,1}^- - (2l+1)H_{l,1}^-\\
&\quad -(l+2)(2l-1)H_{l+2,1}^-]. \qquad (3.18)\\
\tilde{h}_l^{3-} &= \frac{\mu}{\beta}\frac{\sqrt{l(l+1)}\,i^{l+1}}{(2l-1)(2l+1)(2l+3)}\,[2(l^2-1)(2l+3)H_{l-2,1}^- - 3(2l+1)H_{l,1}^-\\
&\quad + 2l(l+2)(2l-1)H_{l+2,1}^-]\\
\tilde{h}_l^{4-} &= \frac{\mu}{\alpha}\frac{2\,i^{l+1}}{(2l-1)(2l+1)(2l+3)}\,[l(l-1)(2l+3)H_{l-2,1}^-\\
&\quad + (l+1)(l+2)(2l-1)H_{l+2,1}^- - q(l)H_{l,1}^-]\\
\tilde{h}_l^{5-} &= \frac{\mu}{\alpha}\frac{2\sqrt{l(l+1)}\,i^{l+1}}{(2l-1)(2l+1)(2l+3)}\,[(l-1)(2l+3)H_{l-2,1}^- - (2l+1)H_{l,1}^-\\
&\quad -(l+2)(2l-1)H_{l+2,1}^-]\\
q(l) &= (2l+1)\left[2l^2+2l-1+\frac{\alpha^2-2\beta^2}{2\beta^2}(2l-1)(2l+3)\right].
\end{aligned} \tag{3.18}$$

For $\mu = 0$, the only surviving term is

$$\tilde{h}_l^{4-} = -\frac{\lambda}{\alpha}H_{l,1}^-\,i^{l+1}.$$

Factors of i^l, i^{l+1} have been introduced so that the functions g_l^{i-}, h_l^{i-} are always real.

4 The coupled integral equations in the time domain

The problem is now reduced to solving the set of coupled integral equations (3.16) subject to the boundary condition (2.10) or (2.8). The apparent traction due to the prestress

$\mathbf{T}(\mathbf{u}^0)\cdot\hat{n}$ can always be expanded in vector spherical harmonics. For simplicity, we consider only subsonic growth starting at time $t = 0$. The integral equations can then be written in the compact form:

$$\sum_{j=1}^{J}\int_0^{t-r/v_j} d\tau\, d^j(\tau)\left[\sum_{n=-1}^{N} K_n^{ij}\frac{g_n(t-\tau-r/v_j)}{r^{n+2}(t)}\right] = T^i r(t). \tag{4.1}$$

Here d^j are the functions to be determined, T^i are the apparent tractions $-\mathbf{T}(\mathbf{u}^0)$, v_j is the velocity appropriate for the vector harmonic associated with d^j and r is the position of the cavity surface. The function g_n is defined by:

$$\begin{aligned} g_n(t) &= \delta(t) \qquad n = -1 \\ &= t^n H(t) \qquad n \geqslant 0. \end{aligned} \tag{4.2}$$

The summation limit J is two for the coupled P–SV case and one for the uncoupled (toroidal or spherically symmetric) cases. The elements K_n^{ij} are constants and are linear combinations of the a_l^s from equation (3.12) determined by the expression for the tractions (equation 3.18). For example, for $l = 0$, the element K_{-1}^{11} is the coefficient of the delta function occurring in h_0^{4-} which from (3.18) and (3.12) is:

$$K_{-1}^{11} = \frac{2\mu i}{-3}\left[-q(0)\,a_0^1 - 2a_2^1\right]. \tag{4.3}$$

To find any given K_n^{ij}, find the coefficient of $g_n(t-x)/r^{n+2}$ in equation (3.12) for l, $l-2$ and $l+2$ and form the linear combinations of (3.18). For the coupled P–SV case use:

$$\begin{bmatrix} K_n^{11} & K_n^{12} \\ K_n^{21} & K_n^{22} \end{bmatrix} = \begin{bmatrix} h_l^{4-} & h_l^{2-} \\ h_l^{5-} & h_l^{3-} \end{bmatrix}.$$

Similarly, for the toroidal case the only non-vanishing term is K_n^{11} which is found using h_l^{1-}. For the coupled P–SV case the i index refers to the $\mathbf{P}_{lm}$ or $\mathbf{B}_{lm}$ components while the j index refers to the $\mathbf{L}_{lm}$ or $\mathbf{N}_{lm}$ eigenvectors. The upper limit N is the largest non-vanishing value of s in the a_l^s coefficients, which will be equal to $l+3$ for the coupled P–SV case and $l+2$ for the toroidal case.

The next step is the numerical solution of equation (4.1). If r were not time dependent, a Fourier or Laplace transform could be applied to (4.1) and the solution would follow from the convolution theorem. Since this is not possible, we use the following direct numerical solution. The time interval of interest is divided into a number of subintervals. In each subinterval a polynomial solution for d^j with unknown coefficients is assumed. The integral in (4.1) can then be evaluated analytically at selected points in the subinterval. A least squares inverse is used to evaluate the unknown coefficients of the polynomial and therefore the d^j at all points within the interval. Further details can be found in Stevens (1980b).

Once the coefficients d^j have been determined, the displacements may be found at any position and time by evaluating equation (3.13) at the observation point. In the notation of this section equation (3.13) may be written for each multipole as:

$$u^i(r,t) = \sum_{j=1}^{J}\int_0^{t-r/v_j} d\tau\, d^j(\tau)\left[\sum_{n=0}^{N}\bar{K}_n^{ij}\frac{g_n(t-\tau-r/v_j)}{r^{n+1}(t)}\right] \tag{4.4}$$

where the coefficients $\bar{K}_n^{ij}$ are again linear combinations of the a_l^s corresponding to $r^{-(n+1)}$ and determined by equation (3.14).

The solution given here is for a source with a very weak material inside the spherical source region. As mentioned before, the solution could be extended to include a liquid or solid material in the source region. This would require the boundary conditions for continuity of normal (liquid) and tangential (solid) displacement to be added to the integral equation (4.1) and would increase the number of simultaneous equations to be solved to three or four for the coupled *P–SV* case.

This solution was made possible by the separability of the vector elastic equations in spherical coordinates. In the usual sense, the number of separable coordinate systems is very limited. The vector elastic equations separate only in spherical and cylindrical coordinates. It would be very useful for a study of spontaneous sources such as earthquakes to be able to separate the equations in other coordinate systems more appropriate to the shape of the source. Wyss (1982) describes a generalization of the method of separation of variables which may make it possible to achieve separation in many more coordinate systems. This would allow the extension of the spherical solutions to other failure geometries.

5 Numerical results

The mathematical technique of the last section may be performed for each multipole independent of the stress field. In order to compute waveforms, it is necessary to specify the prestress (expanded in vector spherical harmonics) and take the corresponding linear combination of multipoles at each angle. The simplest prestress field is uniform compression which can be written

$$\mathbf{T}(\mathbf{u}^0) \cdot \hat{n} = A_{00}\,\mathbf{P}_{00} \tag{5.1}$$

so only the monopole is involved.

A uniform shear stress field can also be written simply using only an $l = 2$ quadrupole field:

$$\mathbf{T}(\mathbf{u}^0) \cdot \hat{n} = \sum_{m=-2}^{+2} A_{2m} \left(\mathbf{P}_{2m} + \frac{\sqrt{6}}{2} \mathbf{B}_{2m} \right) \tag{5.2}$$

where the coefficients A_{2m} depend on the orientation of the prestress field (Stevens 1980a).

The computations of the last section require specification of the growth rate. We consider two types of growth – growth which is linear until it suddenly stops and growth which starts at a prescribed velocity and decreases quadratically to zero. This growth history is described by

$$R = -\frac{V_0^2}{4R_{\max}}\, t \left(t - \frac{4R_{\max}}{V_0} \right) \tag{5.3}$$

where V_0 is the initial velocity and $R_{\max}$ is the ultimate radius which is formed at time

$$t = \frac{2R_{\max}}{V_0}.$$

We first want to compare this numerical solution with the only analytic solution available. Fig. 1 shows the P and S waveforms for a cavity which grows linearly with a velocity of $\beta/2$ in a uniform shear field. The observation point is at $20R_{\max}$. The figures have been scaled to match the figures in Burridge (1975). The waveforms are a very close match to those of Burridge. There is some inaccuracy in the shear wave caused by the abrupt stop of cavity growth which causes an abrupt change in the shear wave coefficient $d^2(\tau)$ making it difficult to match with a polynomial.

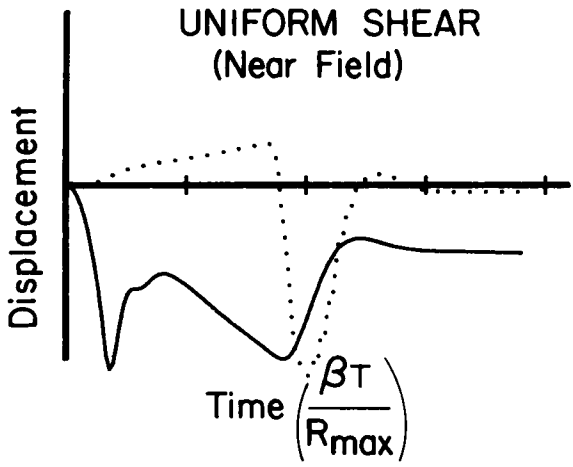

Figure 1. Radial (solid) and tangential (dotted) waveforms for an expanding spherical cavity in a uniform shear field which grows at a velocity of 0.5β and suddenly stops, observed at a distance of $20R_{max}$. The waveforms are scaled for comparison with the analytic solution of Burridge (1975).

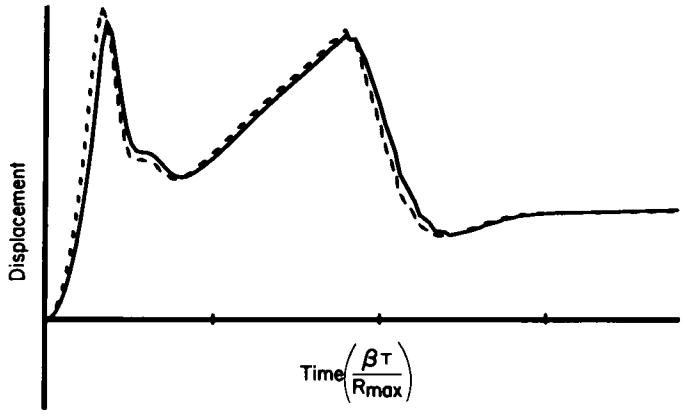

Figure 2. The boundary conditions for a growing cavity depend on the particle velocity within the cavity. 'Cavity', as used here, means a region in which all material strength is lost. The solid line shows the radial displacement for vanishing velocities inside, the dotted for continuous velocities. The resulting differences are quite small.

Fig. 2 shows the effect of the extra term in the boundary condition (equation 2.8) for the same growth conditions as the previous example. The solid line shows the P waveform for vanishing velocities inside so that the boundary condition becomes:

$$\mathbf{T}(\mathbf{u}) \cdot \hat{n} + \rho \frac{\partial \mathbf{u}}{\partial t} \mathbf{U} \cdot \hat{n} = -\mathbf{T}(\mathbf{u}^0) \cdot \hat{n}. \tag{5.4}$$

The dotted line shows the P waveform for continuous velocities. Clearly, the difference is very small. The amplitude of the wave is slightly larger for zero velocities inside, since the momentum is transferred to the exterior region. Nevertheless, neglect of this term (which will usually be undetermined) is not likely to cause a significant error.

The following examples are all for a quadratic growth history with different starting velocities, with cavity radius $R_{max} = 1$, and $\alpha = 3.5$, $\beta = 2$. Tic marks on the figures indicate seconds. All examples are far-field waveforms.

Fig. 3 shows the waveforms from an expanding cavity in a uniform compressive stress field at growth rates of $\beta/2$ (solid) and $\beta/20$ (dashed). The two curves in the top figure are drawn to scale. It is clear that the primary effect of growth is to cause the waveform to be lower in amplitude and longer in duration. In the lower figure the amplitude and time-scales are changed to show the relative shapes of the waveforms. The shapes are very much alike. The main difference is a reduction in the size of the 'overshoot' at the end of the waveform. Note the gradual onset of the waveforms in contrast to the abrupt onset observed in instantaneous problems (e.g. Stevens 1980a).

Fig. 4 shows the P and S waveforms for a uniform shear field with a starting velocity of 0.5β. Again we have a reduction in overshoot – especially in the P-wave and a reduction in the effects of diffraction in the P-wave compared to the instantaneous problem. Fig. 5 shows the P and S waveforms for a slow growth rate of 0.1β. Now the P- and S-waves have almost the same duration (approximately the total growth time) and the effects of diffraction and overshoot are almost eliminated.

Stevens (1980a) found a number of effects which result from failure in an inhomogeneously prestressed medium. The techniques of this section can be used to see if these

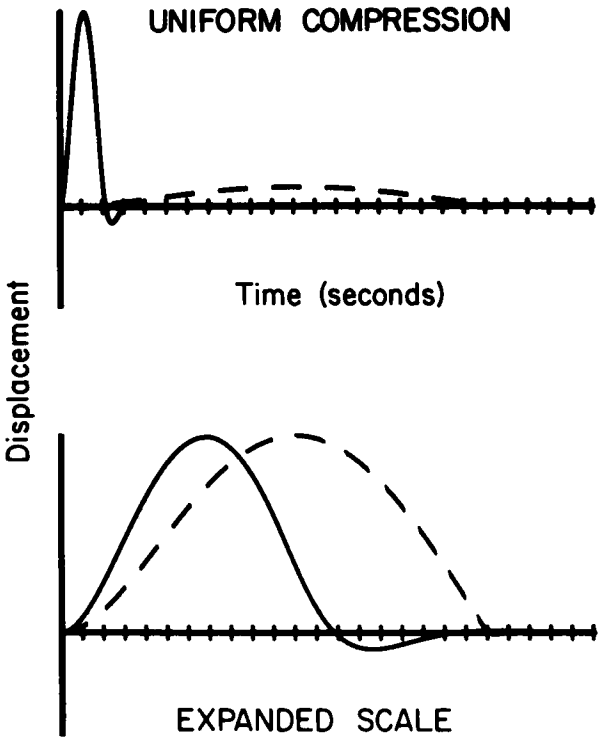

Figure 3. Far-field waveforms for a quadratically expanding spherical cavity in a uniform compressive stress field at two different growth rates. In the solid line, growth starts at a velocity of $\beta/2$; in the dashed line, at $\beta/20$. In the bottom figure, the time-scale is increased by a factor of six for the rapid growth rate, and the amplitude is increased by a factor of 10 for the slow growth rate to show the relative shapes. The shapes of the two waveforms are similar, but the slower growth rate causes a decrease in amplitude and an increase in duration. The area under the pulse remains constant.

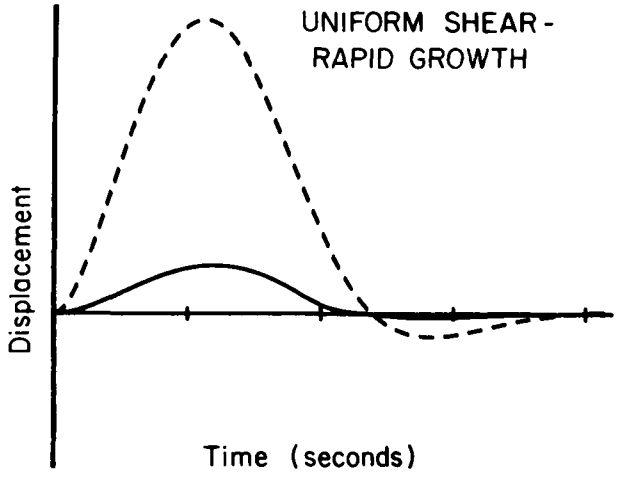

Figure 4. *P* (solid) and *S* (dashed) far-field waveforms from a quadratically expanding spherical cavity in a uniform shear field with a starting velocity of 0.5β.

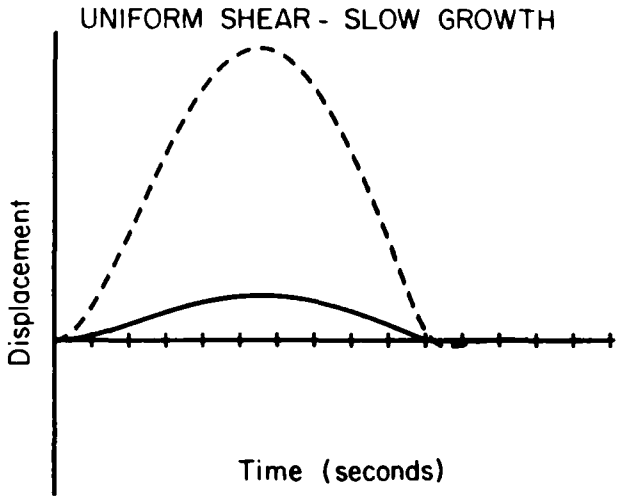

Figure 5. Waveforms for the same conditions as Fig. 4, but with an initial velocity of 0.1β. The overshoot is reduced and the *P*- and *S*-waves have almost the same duration.

effects persist with a finite rupture velocity. The stress field due to a centre of compression at a distance L from the cavity centre can be written:

$$\mathbf{T}(\mathbf{u}^0)\cdot\hat{e}_r = \mu \sum_{l=2}^{\infty} \frac{R^{l-2}}{L^{l+1}} \left[l(l-1)\,\mathbf{P}_{l0} + (l-1)\sqrt{l(l+1)}\,\mathbf{B}_{l0}\right]$$

for the coordinates shown in Fig. 6.

The most obvious and most sensitive effect of an inhomogeneous stress field is the variation in waveform shape with angle. Fig. 7 shows the far-field pulses from a growing cavity (quadratic growth with initial velocity of $\beta/2$) located at $L = 2R_{\max}$ away from a centre of compression. The waveforms are shown for several angles ($\theta = 0$ is the direction of the stress concentration). Fig. 8 shows the pulses for an instantaneously created cavity at the same

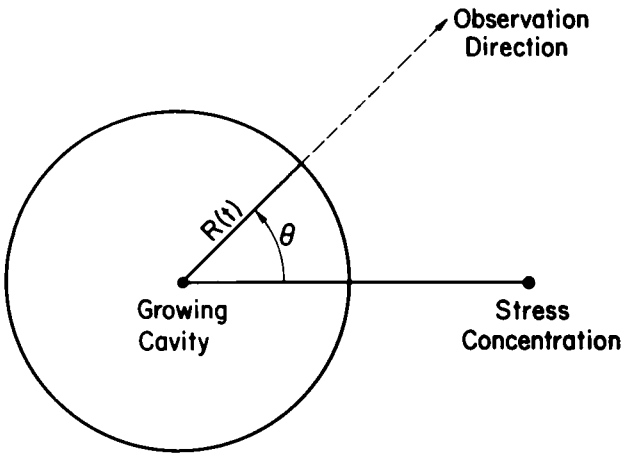

Figure 6. Coordinates for growing spherical cavity with a stress concentration nearby.

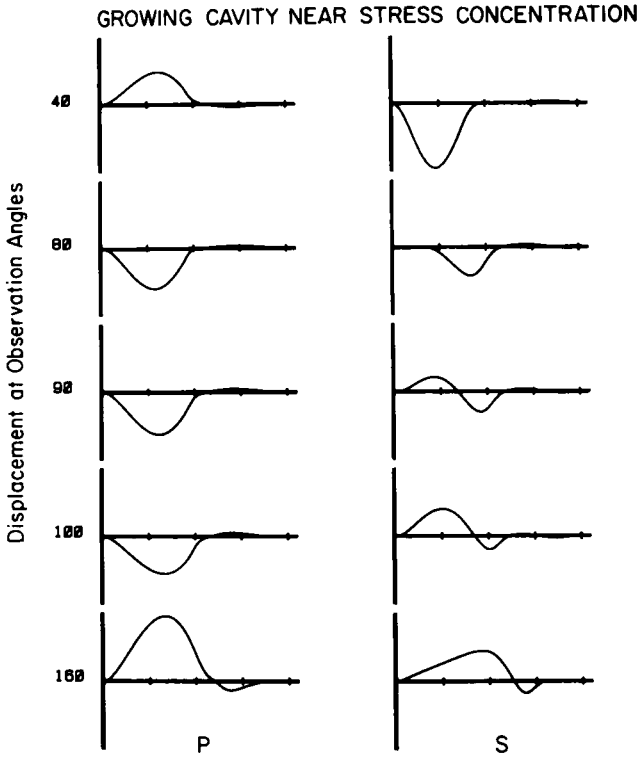

Figure 7. Seismic radiation from a spherical cavity with a quadratic growth history with a centre of compression located two radii from the cavity centre. The *P*-wave is on the left and the *S*-wave is on the right (normalized separately). Comparison with Fig. 8 shows that the first parts of the waveforms are more emergent than in the instantaneous case, but the complexity of the waveforms and the variation of shape with angle still remains. The initial rupture velocity is $0.5\,\beta$.

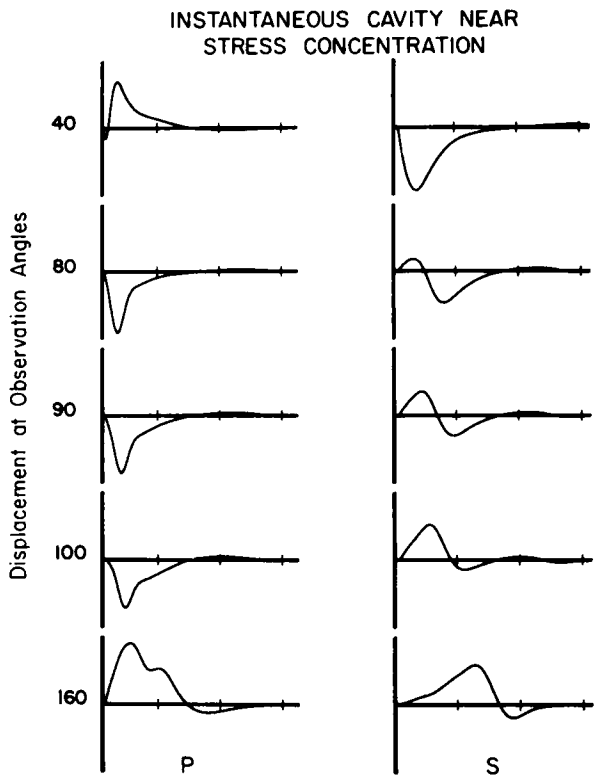

Figure 8. Seismic radiation from the sudden creation of a spherical cavity with a centre of compression two radii from the cavity centre. Notice the variation of pulse shape and arrival time with angle.

location for comparison. Both figures show a pronounced change in waveform shape with angle. In particular, there is a pronounced broadening of the waveform and a delay in arrival time with increasing angle. Near the 'node' at $\theta = 90°$, the shear wave is double sided. The main effect of growth is on the first part of the waveform. The onset of the waveform is more gradual. Also, the effect of diffraction in the last part of the *P*-wave is reduced. The waveforms are longer in duration than the instantaneous waveforms but have much the same shape. The increased complexity of the waveform caused by the inhomogeneous stress field still exists.

6 Conclusions

We have derived a method of solution for the seismic radiation from an arbitrarily growing spherical cavity in an arbitrarily prestressed elastic medium. The problem is formulated as a set of coupled Volterra integral equations. The integral equations are easy to generate and can be used for more general problems than previous formulations in terms of coupled differential equations.

The numerical solution of these equations has been used to compute waveforms for several stress fields and growth rates and has been compared with waveforms from instantaneous cavity formation in the same prestress field. The main effect of the finite growth rate is that the waveforms are spread out over a longer period of time with a corresponding reduction in amplitude but with constant moment. The diffraction which is very evident in far-field *P*-waveforms in the instantaneous problem is reduced. The effects

produced by an in homogeneous stress field, however, are strongly evident for the growing as well as for the instantaneous spherical source. In particular, the shape of the waveforms changes considerably with observation angle around the source. In the direction of a stress concentration, the waveforms are narrower and arrive earlier than waveforms observed at other angles.

Acknowledgment

This work was supported by AFOSR Grant Number F49620-80-C-0018 and Lawrence Livermore Grant Number 4723109.

References

Archambeau, C. B., 1972. The theory of stress wave radiation from explosions in prestressed media, *Geophys. J. R. astr. Soc.*, **39**, 329–366.

Archambeau, C. B. & Minster, J. B., 1978. Dynamics in prestressed media with moving phase boundaries: a continuum theory of failure in solids, *Geophys. J. R. astr. Soc.*, **52**, 65–96.

Ben-Menahem, A. & Singh, J., 1968. Eigenvector expansions of Green's Dyads with applications to geophysical theory, *Geophys. J. R. astr. Soc.*, **16**, 417–452.

Burridge, R., 1969. Spherically symmetric differential equations, the rotation group, and tensor spherical functions, *Proc. Camb. Phil. Soc.*, **65**, 157–175.

Burridge, R., 1975. The pulse shapes and spectra of elastic waves generated when a cavity expands in an initial shear field, *J. geophys. Res.*, **80**, 3606–2607.

Burridge, R., 1976. Reply (to Snoke, 1976), *J. geophys. Res.*, **81**, 1037–1038.

Burridge, R. & Alterman, Z., 1972. The elastic radiation from an expanding spherical cavity, *Geophys. J. R. astr. Soc.*, **30**, 451–477.

Hirasawa, T. & Sato, R., 1963. Propagation of elastic waves from a spherical origin: parts 1 and 2 (in Japanese) *Zisin*, **16**, 52–77.

Koyama, J., Horiuchi, S. E. & Hirasawa, T., 1973. Elastic waves generated from sudden vanishing of rigidity in a spherical region, *J. Phys. Earth*, **21**, 213–226.

Minster, J. B., 1979. Near-field waveforms from an arbitrarily expanding, transparent spherical cavity in a prestressed medium, *Geophys. J. R. astr. Soc.*, **56**, 81–96.

Minster, J. B. & Suteau, A., 1977. Far-field waveforms from an arbitrarily expanding transparent spherical cavity in a prestressed medium, *Geophys. J. R. astr. Soc.*, **50**, 215–233.

Stevens, J. L., 1980a. Seismic radiation from the sudden creation of a spherical cavity in an arbitrarily prestressed elastic medium, *Geophys. J. R. astr. Soc.*, **61**, 303–328.

Stevens, J. L., 1980b. Seismic stress relaxation phenomena in an inhomogeneously prestressed medium, *PhD thesis*, University of Colorado, Boulder, Colorado.

Wyss, R. K., 1982. Generalized separability, *J. math. Phys.*, submitted.

Appendix: equivalence of vector harmonics and generalized harmonics

Burridge (1969) defines the generalized spherical harmonics by

$$Y_l^{Nm}(\theta,\phi) = P_l^{Nm}(\cos\theta)\exp(im\phi)$$

$$P_l^{Nm}(\mu) = \frac{(-1)^{l-N}}{2^l(l-N)!}\sqrt{\frac{(l-N)!\,(l+m)!}{(l+N)!\,(l-m)!}}\,(1-\mu)^{-1/2(m-N)}(1+\mu)^{-1/2(m+N)}$$
$$\times\frac{d^{l-m}}{d\mu^{l-m}}(1-\mu)^{l-N}(1+\mu)^{l+N}.$$

For $N = 0$ this reduces to the scalar harmonic Y_{lm}. The vector harmonic $\mathbf{P}_{lm}$ is defined by:

$$\mathbf{P}_{lm} = Y_l^{0m}(\theta,\phi)\,\hat{e}_r.$$

We make use of the recursion relations

$$\Omega_N P_l^{N-1,m}(\cos\theta) - \Omega_{N+1} P_l^{N+1,m}(\cos\theta) = \sqrt{2}\,\frac{d}{d\theta} P_l^{Nm}(\cos\theta)$$

and

$$\Omega_N P_l^{N-1,m}(\cos\theta) + \Omega_{N+1} P_l^{N+1,m}(\cos\theta) = \sqrt{2}\,\frac{N\cos\theta - m}{\sin\theta} P_l^{Nm}(\cos\theta)$$

where

$$\Omega_N = \sqrt{\frac{(l+N)(l-N+1)}{2}}.$$

Combining, we get

$$\sqrt{(l+N)(l-N+1)}\,P_l^{N-1,m}(\cos\theta) = \left[\frac{N\cos\theta - m}{\sin\theta} + \frac{d}{d\theta}\right] P_l^{Nm}(\cos\theta)$$

and

$$\sqrt{(l+N+1)(l-N)}\,P_l^{N+1,m}(\cos\theta) = \left[\frac{N\cos\theta - m}{\sin\theta} - \frac{d}{d\theta}\right] P_l^{Nm}(\cos\theta).$$

Setting $N = 0$ we get

$$\sqrt{l(l+1)}\,P_l^{-1m}(\cos\theta) = \left[\frac{-m}{\sin\theta} + \frac{d}{d\theta}\right] P_l^{0m}(\cos\theta)$$

$$\sqrt{l(l+1)}\,P_l^{1m}(\cos\theta) = \left[\frac{-m}{\sin\theta} - \frac{d}{d\theta}\right] P_l^{0m}(\cos\theta).$$

We compare this with Ben-Menahem & Singh's definition:

$$\sqrt{l(l+1)}\,\mathbf{B}_{lm} = \left[\hat{e}_\theta \frac{\partial}{\partial\theta} + \hat{e}_\phi \frac{im}{\sin\theta}\right] P_l^{0m}\exp(im\phi)$$

$$\sqrt{l(l+1)}\,\mathbf{C}_{lm} = \left[\hat{e}_\theta \frac{im}{\sin\theta} - \hat{e}_\phi \frac{\partial}{\partial\theta}\right] P_l^{0m}\exp(im\phi).$$

The result is

$$\mathbf{B}_{lm} + i\mathbf{C}_{lm} = [\hat{e}_\theta - i\hat{e}_\phi]\,P_l^{-1m}(\cos\theta)\exp(im\phi)$$
$$\mathbf{B}_{lm} - i\mathbf{C}_{lm} = -[\hat{e}_\theta + i\hat{e}_\phi]\,P_l^{1m}(\cos\theta)\exp(im\phi).$$

Conversely

$$\mathbf{B}_{lm} = \frac{1}{2}\hat{e}_\theta\,(P_l^{-1m} - P_l^{1m})\exp(im\phi) - \frac{1}{2}\hat{e}_\phi\,(P_l^{-1m} + P_l^{1m})\exp(im\phi)$$

$$\mathbf{C}_{lm} = \frac{1}{2i}\hat{e}_\theta\,(P_l^{-1m} + P_l^{1m})\exp(im\phi) - \frac{1}{2}\hat{e}_\phi\,(P_l^{-1m} - P_l^{1m})\exp(im\phi).$$